

Article

# In Vitro Toxicity of TiO<sub>2</sub>:SiO<sub>2</sub> Nanocomposites with Different Photocatalytic Properties

Rossella Bengalli <sup>1,\*</sup>, Simona Ortelli <sup>2</sup> , Magda Blosi <sup>2</sup>, Anna Costa <sup>2</sup>, Paride Mantecca <sup>1</sup>  and Luisa Fiandra <sup>1</sup>

<sup>1</sup> POLARIS Research Centre, Department of Earth and Environmental Sciences, University of Milano—Bicocca, Piazza della Scienza 1, 20126 Milano, MI, Italy

<sup>2</sup> Institute of Science and Technology for Ceramics (CNR-ISTEC), National Research Council of Italy, Via Granarolo 64, 48018 Faenza, RA, Italy

\* Correspondence: rossella.bengalli@unimib.it; Tel.: +39-02-64483406

Received: 18 June 2019; Accepted: 17 July 2019; Published: 21 July 2019



**Abstract:** The enormous technological relevance of titanium dioxide (TiO<sub>2</sub>) nanoparticles (NPs) and the consequent concerns regarding potentially hazardous effects that exposure during production, use, and disposal can generate, encourage material scientists to develop and validate intrinsically safe design solution (safe-by-design). Under this perspective, the encapsulation in a silica dioxide (SiO<sub>2</sub>) matrix could be an effective strategy to improve TiO<sub>2</sub> NPs safety, preserving photocatalytic and antibacterial properties. In this work, A549 cells were used to investigate the toxic effects of silica-encapsulated TiO<sub>2</sub> having different ratios of TiO<sub>2</sub> and SiO<sub>2</sub> (1:1, 1:3, and 3:1). NPs were characterized by electron microscopy and dynamic light scattering, and cell viability, oxidative stress, morphological changes, and cell cycle alteration were evaluated. Resulting data demonstrated that NPs with lower content of SiO<sub>2</sub> are able to induce cytotoxic effects, triggered by oxidative stress and resulting in cell necrosis and cell cycle alteration. The physicochemical properties of NPs are responsible for their toxicity. Particles with small size and high stability interact with pulmonary cells more effectively, and the different ratio among silica and titania plays a crucial role in the induced cytotoxicity. These results strengthen the need to take into account a safe(r)-by-design approach in the development of new nanomaterials for research and manufacturing.

**Keywords:** nanoparticles; safe(r)-by-design; in vitro toxicity

## 1. Introduction

Nanotechnology is growing tremendously fast, and it has led to the creation of a new class of materials, called nanomaterials (NMs), which are nowadays present in everyday life goods. In particular, metal oxide nanoparticles (NPs), thanks to their several properties (antibacterial, photocatalytic, etc.) [1,2] are gaining great attention. Nevertheless, there is a growing concern about the safety of these NMs, due to the increasing release in the market and their consequent intentional and unintentional emission into the environment. In this perspective, to guarantee a sustainable development of these new technologies, the environmental and health safety issues should be addressed in parallel.

Titanium dioxide (TiO<sub>2</sub>) is largely used as a white pigment in the production of several manufacturing (paint, ceramics, textiles, dental care products, etc.) thanks to its ability to strongly adsorb ultraviolet (UV) lights. Under UV light irradiation, the physical properties of TiO<sub>2</sub> change, promoting the decomposition of organic and inorganic compounds. For these properties, TiO<sub>2</sub> is highly employed as a photocatalytic agent in a variety of applications, such as pollution remediation in air and water, sterilization, and production of self-cleaning surfaces. Photocatalyzed TiO<sub>2</sub> nanoparticles (NPs)

have been thoroughly examined given their potential application in cancer therapies and their ability in eradicating cancer cells depends on particle concentrations, cell types, and surface chemistry [3]. Recently, TiO<sub>2</sub> NPs have been identified as efficient sensitizers for photodynamic and sonodynamic cancer therapy, especially upon functionalization with antibodies aimed to optimize the selective distribution to target cells [4].

TiO<sub>2</sub> nanoparticles (NPs), which are also commonly used in food coloring and packaging, cosmetic and oral care products have recently been investigated as efficient antimicrobial agents. TiO<sub>2</sub> NPs have long been known as efficient antimicrobial agents [5]. The photocatalytic properties of TiO<sub>2</sub> NPs depend on its crystalline structure, with the anatase crystalline structure having the highest photocatalytic activity [6,7], and on particle size and specific surface area (the smaller the particle size, the greater the number of active surface sites, and the surface charge-carrier-transfer rate increases in photocatalysis). It has been previously demonstrated that TiO<sub>2</sub> nanoparticles' complexation with silica (SiO<sub>2</sub>) increases TiO<sub>2</sub> photocatalytic activity on self-cleaning textiles, proportionally related to SiO<sub>2</sub> content. The higher photocatalytic effect has been ascribed to an increase of titanium surface acidity that, in turn, affected its hydrophilicity [8].

The issue of TiO<sub>2</sub> toxicity is a crucial aspect to be considered for its application as a photocatalytic agent in self-cleaning surfaces. Even if over the last decades the research activity on the toxicity of TiO<sub>2</sub> NPs has been strongly improved, questions about the safe use of these nanoparticles are still open. As photocatalytic activation of TiO<sub>2</sub> induces a greater generation of reactive oxygen species (ROS), so it is likely that this also improves its toxicological potential. Some reports from the literature have shown that TiO<sub>2</sub> is toxic in the presence of UV irradiation due to ROS generation [9]. UV irradiation of TiO<sub>2</sub> suspensions can also change the state of agglomeration of the nanoparticles affecting their photocatalytic activities [10] with an indirect impact on cell viability. Several in vitro studies evidenced that a certain toxicity and genotoxicity is associated with the exposure to TiO<sub>2</sub> NPs even in the absence of photoactivation. Oxidative stress is the main toxicity mechanism for non-photoactivated NPs also, with alteration of mitochondrial functionality and induction of DNA damage in different human and non-human cell lines [11–13].

The surface functionalization of TiO<sub>2</sub> NPs with SiO<sub>2</sub>, resulting in an increase of hydrophilicity, not only was demonstrated to be able to improve their photocatalytic potential on textile surfaces [8] but also to affect their biocompatibility. TiO<sub>2</sub> NPs encapsulation in a SiO<sub>2</sub> matrix was demonstrated to be an effective solution to control the redox reactivity of TiO<sub>2</sub> NPs by reducing ROS production [14]. Nevertheless, the toxic effects on live cells, as a function of encapsulating SiO<sub>2</sub> content, have limited investigations. NPs photocatalyst performance is related to the ratio TiO<sub>2</sub>:SiO<sub>2</sub> in the nanocomposites, which can also be responsible for different cellular consequences upon direct exposure to these new nanomaterials (NMs).

Recently, studies and development of hybrid and core@shell NPs, nanocomposites, and layer-by-layer NPs have arisen [15–18]. Since these new NMs have different properties from their single NPs constituents, concern and research about their safety are increasing in parallel, pointing out the importance of investigating NPs toxicity in a perspective of sustainable nanotechnology. This study aims to compare the different biological effects induced by silica-encapsulated TiO<sub>2</sub> [19], comparing different SiO<sub>2</sub> content (TiO<sub>2</sub>/SiO<sub>2</sub> ratio). The effects of the different nanocomposites were tested against the human lung epithelial cells A549, that have been demonstrated as being a good target for the safety assessment of titania NPs [13,20]. Furthermore, A549 cells, derived from a human adenocarcinoma of the lung, are the most often used cell line for toxicity testing. The cells show properties such as surfactant production and transport=like AT-II cells in vivo, secrete cytokines, and perform phase I and phase II xenobiotic biotransformation similar to lung tissue [21,22]. Furthermore, it is important to select the cell line which best represents the intended exposure route, and in this perspective, A549 cells are used for the screening of nanoparticles in inhalation toxicology. Finally, in the context of the NANoREG framework for the safety assessment of NMs [23], A549 cells were used as the main model

common for several biological endpoints, making this cell line a promising candidate as a cellular model for in vitro testing of NMs at the regulatory level.

The obtained results are of great importance in the selection of the best SiO<sub>2</sub>-modified TiO<sub>2</sub> photocatalysts, matching safe-by-design requirements.

## 2. Materials and Methods

### 2.1. Materials

The following commercial materials were used to prepare the TiO<sub>2</sub>:SiO<sub>2</sub> samples: TiO<sub>2</sub> colloidal nanosuspension (nanosol) containing 6 wt % titania (Colorobbia Italia SpA, Sovigliana Vinci, Italy) and SiO<sub>2</sub> colloidal nanosol, Ludox HS-40<sup>®</sup> containing 40 wt % silica (Grace Davison, Columbia, MD, USA). Dowex<sup>®</sup> 66 anionic exchange resin was purchased from Sigma-Aldrich (Saint Louis, MO, USA).

### 2.2. TiO<sub>2</sub>:SiO<sub>2</sub> Nanosuspensions Preparation

The commercial TiO<sub>2</sub> and SiO<sub>2</sub> nanosols, after appropriate dilution with distilled water, were mixed in well-defined ratios and ball milled for 24 h (zirconia balls with 5 mm diameter). Weight ratios of 1:1, 1:3, and 3:1 were investigated for TiO<sub>2</sub>:SiO<sub>2</sub> NPs. The TiO<sub>2</sub>:SiO<sub>2</sub> samples were mixed at opposite surface charge conditions to promote colloidal heterocoagulation [24]. The obtained samples were basified by anionic exchange resin until a pH of 5 to be more compatible with biological targets. The nanocomposites obtained by the colloidal approach were named TiO<sub>2</sub>:SiO<sub>2</sub> 1:1, TiO<sub>2</sub>:SiO<sub>2</sub> 1:3, and TiO<sub>2</sub>:SiO<sub>2</sub> 3:1 and characterized by a TiO<sub>2</sub> content equal to 0.75 wt %.

### 2.3. TiO<sub>2</sub>:SiO<sub>2</sub> Nanoparticles Characterization

The TiO<sub>2</sub>:SiO<sub>2</sub> nanosols underwent morphological analysis using the FEI Titan transmission electron microscope (TEM) operating at an acceleration voltage of 300 kV (FEI Company, Hillsboro, OR, USA). One drop of the nanoparticle suspension diluted in deionized water (75 µg/mL) was deposited on a film-coated copper grid and characterized.

To perform the identification of crystalline phases, TiO<sub>2</sub>:SiO<sub>2</sub> 1:1, TiO<sub>2</sub>:SiO<sub>2</sub> 1:3, and TiO<sub>2</sub>:SiO<sub>2</sub> 3:1 samples were dried at T° = 100 °C for 3 h in an oven. The obtained powders were characterized by X-ray diffraction (XRD) using a Bragg–Brentano diffractometer (Bruker D8 Advance, Karlsruhe, Germany) operating in a  $\theta/2\theta$  configuration, with an X'Celetor detector LynkEye (10°–80° 2 $\theta$  range, 0.02 step size, 0.5 s per step).

To investigate the colloidal behavior of TiO<sub>2</sub>:SiO<sub>2</sub> NPs in water, hydrodynamic diameter (z-average) and zeta potential ( $\zeta$ -potential) were measured by dynamic light scattering (DLS) and electrophoretic light scattering (ELS) measurements, respectively, using Zetasizer Nanoseries apparatus (Malvern Instruments, Malvern, UK).

### 2.4. Cells Culture Maintenance and Treatments

The A549 cell line (ATCC<sup>®</sup> CCL-185<sup>™</sup>) was routinely maintained as previously reported in Gualtieri and colleagues [25]. Briefly, cells were maintained in OptiMEM medium (Gibco, Life Technologies) supplemented with fetal bovine serum (Gibco, Life Technologies, Monza, Italy) 10% and Pen/Strep 1% (Euroclone, Pero, Italy) at 37 °C, 5% CO<sub>2</sub>.

For the treatments with the different TiO<sub>2</sub>:SiO<sub>2</sub> NPs, cells were seeded in 6 MW (Corning) at the density of 1.5\*10<sup>5</sup> cells/well and incubated until they attached and reached to the confluence of 80% (about 24 h). Cells were treated with NPs for 24 h in all experiments, except for cytofluorimetric analysis (ROS and uptake) in which they were exposed for 180 min (3 h). Each experiment included negative control (untreated cells) and positive control (1 mM H<sub>2</sub>O<sub>2</sub> for ROS detection). For the cell viability experiments, cells were treated with different doses of TiO<sub>2</sub> (7.5, 75, and 750 µg TiO<sub>2</sub>/mL), while for the other experiment, a dose of 75 µg TiO<sub>2</sub>/mL was used.

### 2.5. Cell Viability

The cytotoxicity of TiO<sub>2</sub>:SiO<sub>2</sub> was evaluated through two different analysis: by the 3-(4,5-dimethylthiazol-2-yl)-2,5-diphenyltetrazolium bromide (MTT) test and Hoechst 33342/propidium iodide (H/PI) staining.

MTT (Sigma Aldrich, Milano, Italy) assay was performed according to previous works [26]. Briefly, after 24 h of exposure to NPs, supernatants were collected, centrifuged at 1200 rpm for 6 min, and stored at −80 °C. Cells were rinsed with phosphate buffered saline (PBS), and MTT solution was added to the medium (final concentration 0.3 mg/mL) for 2 h. After the formazan crystal, which are the MTT reduction products, were dissolved in 1 mL Dimethyl sulfoxide (DMSO, Sigma Aldrich), absorbance was analyzed at 570 nm by a multi-plate reader (Infinite 200 Pro, TECAN, Männedorf, Switzerland).

The H/PI nuclear staining allowed to count the number of viable, necrotic, apoptotic, and mitotic A549 cells after NPs exposure. Cells were detached by trypsinization and then re-suspended in a complete medium; 10 µL of 1:1 solution of Hoechst 33342/PI (Sigma Aldrich) was added to cell suspensions and stored in the dark for 15 to 30 min at room temperature. Cells were then centrifuged for 6 min at 1200 rpm, and re-suspended in 20 µL of FBS. Three drops (about 4 µL) of cell suspensions were smeared on a coverslip and observed under a fluorescence microscope (Zeiss-Axioplan, Carl Zeiss Microscopy GmbH, Jena, Germany) with a UV filter (365 nm). At least 300 cells per sample were scored according to nuclei staining and plasma membrane integrity as viable normal cells (H positive and PI negative, without special nuclear characteristic and an intact plasma membrane), necrotic cells (non-apoptotic and PI positive), apoptotic cells (bright H or PI positive stained with condensed or fragmented nuclei), mitotic cells (H positive with chromosome condensation).

### 2.6. Cytological Observation

For morphological analysis, cells were seeded on a cover slide at a concentration of  $1.5 \times 10^5$  cells/well, cultured for 24 h and then exposed to NPs for further 24 h. At the end of the treatment, cells were processed for hematoxylin-eosin (HE) staining, as previously described in [27]. The slides were observed on an optical microscope (Zeiss-Axioplan, Carl Zeiss Microscopy GmbH, Jena, Germany), and pictures were acquired using an AxioCam MRC5 digital camera and processed using AxioVision Real 4.8 software (Carl Zeiss Solutions, Jena, Germany).

Cytoskeleton organization was instead analyzed by staining actin microfilaments with rhodamin phalloidine (1:40 dilution, Cytoskeleton Inc., Denver, CO, USA). Cells, seeded on a cover slide, after exposure to 75 µg/mL of NPs, were fixed in 4% paraformaldehyde for 20 min, washed and permeabilized with 0.1% Triton-100X and then incubated with rhodamin phalloidine for 30 min. After PBS washing, slides were mounted with ProLong™ Gold Antifade Mountant with DAPI (Molecular Probe, Life Technologies, Monza, Italy), dried overnight and then observed under the inverted microscope AxioObserver Z1 Cell Imaging station (Carl-ZEISS Spa, Milano, Italy) and images were acquired by an MRC5 digital camera and elaborated with the dedicated software ZEN 2.3 Blue edition.

### 2.7. Cytofluorimetric Analysis

Cytofluorimetric analyses were performed: (i) to evaluate TiO<sub>2</sub>:SiO<sub>2</sub> NPs capability to induce ROS formation, (ii) to investigate the interaction between different NPs with A549 cells by the side scatter analysis, and (iii) to analyze cell cycle alterations.

For ROS detection, A549 cells were pre-incubated for 20 min with the probe Carboxy-2',7'-Dichlorofluorescein Diacetate (carboxy-DCFDA, 5 µM, Life Technologies) and incubated with NPs for 180 min. After incubation, cells were detached, centrifuged at 1200 rpm for 6 min, re-suspended in 500 µL of PBS and analyzed in the FITC channel by flow cytometry (CytoFLEX, Beckman Coulter GmbH, Krefeld, Germany) with the software CytoExpert. The signal from unloaded samples (cells without the probe carboxy-DCFDA) was evaluated as reference to assess cells and NPs' autofluorescence. These values were then subtracted from the values to DCFDA stained samples.

To investigate the effects on cell cycle, untreated and cells treated for 24 h were harvested, fixed in ethanol 90% and stored at  $-20\text{ }^{\circ}\text{C}$  until analysis. Cells were then centrifuged at 1600 rpm for 6 min, ethanol was discharged, and cells suspended in PBS containing RNAsi-DNasi free (10  $\mu\text{L}$ ) for 30 min at  $37\text{ }^{\circ}\text{C}$ . Then 5  $\mu\text{L}$  of Propidium Iodide (PI) was added for 7 min and finally, cells analyzed by the Cytoflex in the ECD-channel ( $\lambda_{\text{Exc}}$  488 nm,  $\lambda_{\text{Em}}$  610/20 nm). The percentage of cells in the different cell cycle phase (G0, G1, S, and G2/M) was displayed. The side scatter (SSC) was also analyzed to assess cell–NP interaction.

Furthermore, the capability of the different NPs to induce autophagy was assessed through the analysis of LC3B II expression by cytofluorimeter. Cells, after 24 h of exposure to 75  $\mu\text{g}/\text{mL}$  of NPs, were harvested, fixed with paraformaldehyde 4% for 15 min, permeabilized with methanol 90%, and then stained with the antibody rabbit anti-human LC3BII (1:400 dilution, Cell Signaling). After 1 h of incubation in the appropriate buffer (0.5% bovine serum albumin in PBS 1X), cells were washed twice in buffer and then incubated for 30 min with secondary antibody AlexaFluor anti-rabbit 488 (1:200 dilution, Life Technologies). After washing, cells were resuspended in PBS and read by the CytoFLEX in the FITC channel.

## 2.8. Statistical Analysis

The data represent the mean  $\pm$  standard error of the mean (SEM) of at least three independent experiments. Statistical analyses were performed using Sigma Stat 3.2 software, using unpaired *t*-test or one-way ANOVA and Bonferroni's post hoc analysis. Values of  $p < 0.05$  were considered statistically significant.

## 3. Results

### 3.1. $\text{TiO}_2:\text{SiO}_2$ Nanocomposites Characterization

#### 3.1.1. Transmission Electron Microscopy (TEM)

The TEM micrographs (Figure 1) showed aggregated samples with  $\text{TiO}_2$  randomly distributed within a silica matrix. This matrix encapsulation structure is typical of the colloidal heterocoagulation method used to prepare  $\text{TiO}_2:\text{SiO}_2$  samples [19,28]. The energy-dispersive X-ray (EDX) line scan analysis of the elemental distribution, on  $\text{TiO}_2:\text{SiO}_2$  1:1 sample, confirmed the presence of a matrix encapsulation structure, where the  $\text{TiO}_2$  NPs were surrounded by  $\text{SiO}_2$  NPs (Figure 2).

Data on  $\text{TiO}_2$  and  $\text{SiO}_2$  NPs morphology are shown in Supplementary materials (Figure S1).

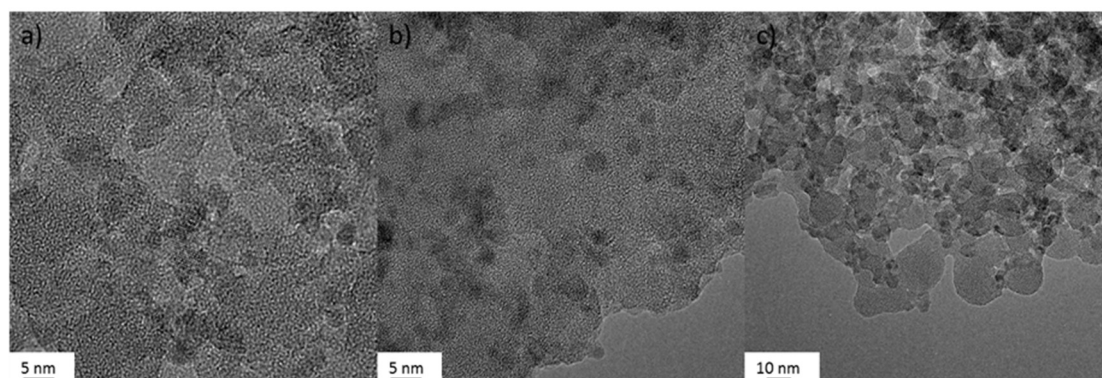


**Figure 1.** TEM images of  $\text{TiO}_2:\text{SiO}_2$  sample: (a)  $\text{TiO}_2:\text{SiO}_2$  1:1, (b)  $\text{TiO}_2:\text{SiO}_2$  1:3, (c)  $\text{TiO}_2:\text{SiO}_2$  3:1.

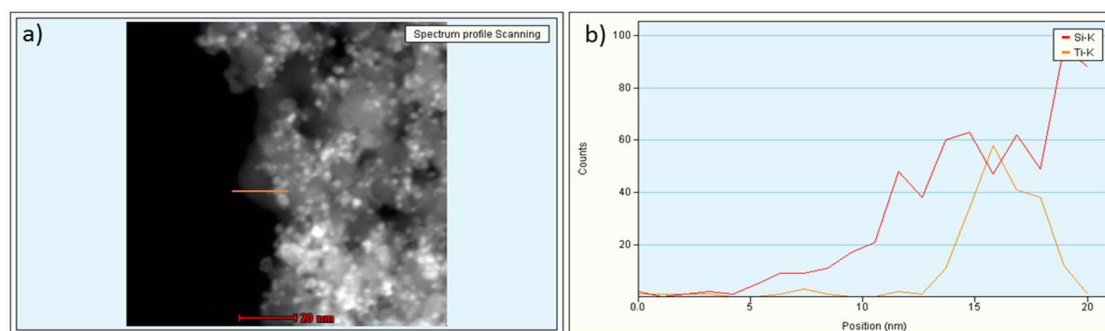


**Figure 2.** EDX-STEM analysis on the  $\text{TiO}_2\text{:SiO}_2$  1:1 sample: (a) sample area analyzed; (b) Si and Ti distribution within the selected area confirm the phase gradient represented in the sketch.

### 3.1.2. Colloidal Properties

Data about the hydrodynamic behavior, PDI and  $\zeta$ -potential values of  $\text{TiO}_2\text{:SiO}_2$  NPs are reported in Table 1. As expected,  $\text{TiO}_2$  (+38 mV) and  $\text{SiO}_2$  (−43 mV) NPs were positively and negatively charged, respectively, at natural pH in water. Their opposite surface charge triggers the heterocoagulation phenomenon, which, by means of electrostatic interactions, promotes the encapsulation of  $\text{TiO}_2$  NPs into the  $\text{SiO}_2$  matrix. The small size, low polydispersity index (PDI) and high values of zeta-potential demonstrated the good colloidal stability of both starting NPs suspensions. The increase of hydrodynamic diameter as a function of the  $\text{TiO}_2\text{:SiO}_2$  ratio is caused by both the steric hindrance of  $\text{SiO}_2$  heterocoagulated on the  $\text{TiO}_2$  surface and the consequent electrostatic destabilization due to the progressive neutralization of the  $\text{TiO}_2$  surface charge with the increase of  $\text{SiO}_2$  content [29,30]. The hydrodynamic diameters showed that  $\text{TiO}_2\text{:SiO}_2$  NPs 1:1 and 3:1 have similar behavior, with average values of 126 and 148 nm, respectively. On the other hand, the hydrodynamic diameter of the sample  $\text{TiO}_2\text{:SiO}_2$  1:3 was much larger than the other NPs (1490 nm) evidencing its tendency to aggregate in an aqueous medium. Moreover,  $\text{TiO}_2\text{:SiO}_2$  1:3 also showed the highest PDI, consistent with a very broad size distribution. Such a different behavior among the samples was well expressed by the zeta potential values. A positively charged surface of the NPs was measured for all the heterocoagulated suspensions. The zeta potentials of  $\text{TiO}_2$ ,  $\text{TiO}_2\text{:SiO}_2$  1:1 and  $\text{TiO}_2\text{:SiO}_2$  3:1, higher than +35 mV, pointed out that these suspensions are stable. On the contrary  $\text{TiO}_2\text{:SiO}_2$  1:3 exhibited a low  $\zeta$ -potential value (<+10 mV), meaning that the electrostatic repulsion barrier cannot prevent flocculation and coagulation phenomena.

**Table 1.** Colloidal properties of NPs. Hydrodynamic diameter (Z-average), polydispersity index (PDI) and zeta potential ( $\zeta$ -potential) of  $\text{TiO}_2\text{:SiO}_2$  nanoparticles (NPs) in water.

Sample	pH	$d_{\text{DLS}}$ (nm)	PDI	Zeta-pot <sub>ELS</sub> (mV)
$\text{SiO}_2$	9.0	$20.4 \pm 0.3$	0.2	$-42.9 \pm 1.1$
$\text{TiO}_2$	1.5	$53.0 \pm 0.9$	0.2	$+38.3 \pm 1.8$
$\text{TiO}_2\text{:SiO}_2$ 1:1	5.0	$125.7 \pm 1.26$	0.4	$+40.5 \pm 0.3$
$\text{TiO}_2\text{:SiO}_2$ 1:3	5.0	$1490.3 \pm 829$	0.8	$+7.08 \pm 0.4$
$\text{TiO}_2\text{:SiO}_2$ 3:1	5.0	$147.8 \pm 2.3$	0.3	$+46.1 \pm 0.3$

### 3.1.3. XRD-Analysis

Figure 3 shows the XRD patterns for  $\text{TiO}_2\text{SiO}_2$  3:1,  $\text{TiO}_2\text{SiO}_2$  1:1 and  $\text{TiO}_2\text{SiO}_2$  1:3 powder samples. The samples show a broad band centered at  $2\theta = 22.0$ , the characteristic peak for amorphous  $\text{SiO}_2$  (JCPDS 29–0085) with an intensity proportional to the amount of silica added. Anatase (JCPDS 21–1272) is the predominant crystalline phase of  $\text{TiO}_2$  component, then there are small amounts of brookite (JCPDS 29–1360) and rutile (JCPDS 65–0190). In general, broad peaks are present, they are typical of nano-sized crystallites.

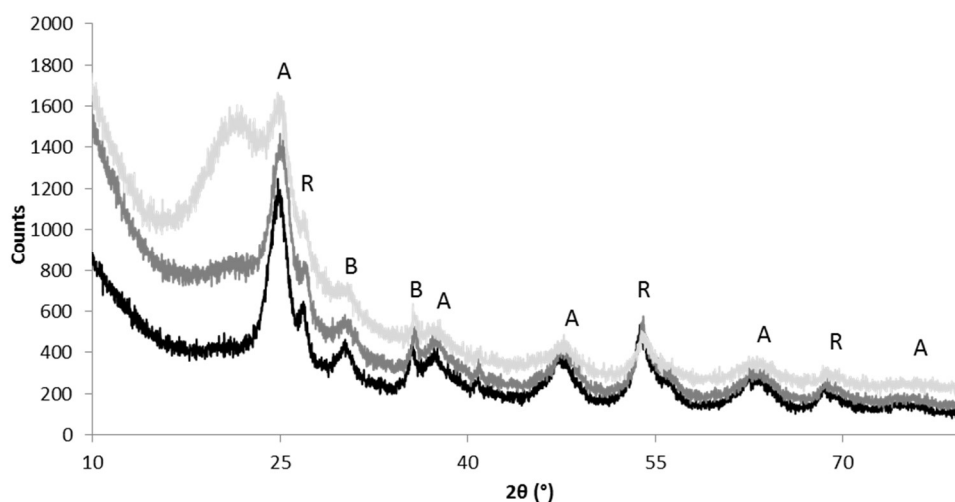


**Figure 3.** X-ray diffractograms of TiO<sub>2</sub>SiO<sub>2</sub> 3:1 (black), TiO<sub>2</sub>SiO<sub>2</sub> 1:1 (medium gray) and TiO<sub>2</sub>SiO<sub>2</sub> 1:3 (light gray). (A = anatase; B = brookite; R = rutile).

### 3.2. Cytotoxicity

#### 3.2.1. Cell Viability: MTT Test and H/PI

Cells viability was assessed to evaluate the toxic potential of TiO<sub>2</sub> based nanocomposites. Data from MTT test showed that particles TiO<sub>2</sub>:SiO<sub>2</sub> 3:1, with a lower amount of SiO<sub>2</sub> vs. TiO<sub>2</sub>, have affected the viability of the cells at the doses 750 and 75 µg/mL with a mortality of the 30% and 10%, respectively (Figure 4a). Cell viability data obtained from the exposure to TiO<sub>2</sub> and SiO<sub>2</sub> NPs alone are reported in Supplementary Materials (Figure S2). To investigate the type of cell death induced by these NPs, H/PI staining has been performed at the dose 75 µg TiO<sub>2</sub>/mL, which is the dose used for the other endpoints. Furthermore, this effective concentration falls in the range (from 1 µg/mL until 200 µg/mL) recommended for the in vitro testing of NMs aiming to investigate biological responses and in mechanistic studies [31,32]. Results from this test showed that TiO<sub>2</sub>:SiO<sub>2</sub> 3:1 induced a reduction of cell viability, as demonstrated by the increased number of necrotic cells (Figure 4b). Results on TiO<sub>2</sub> NPs alone are reported in the Supplementary Materials (Figure S3a).

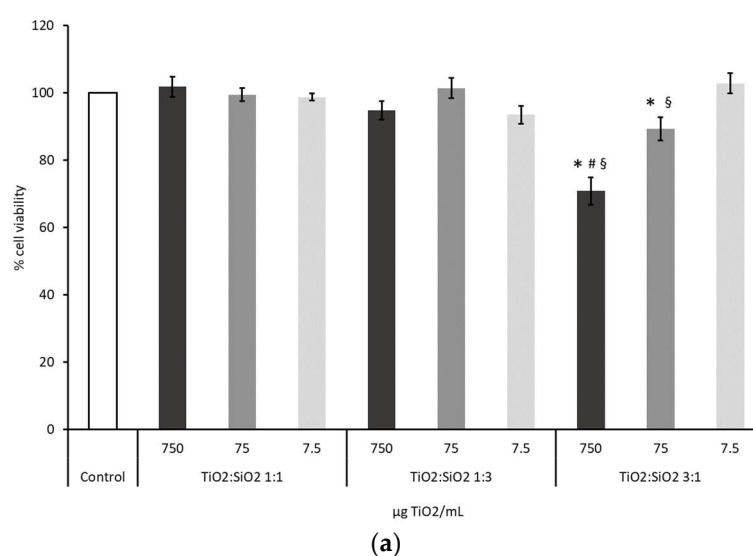


**Figure 4.** Cont.

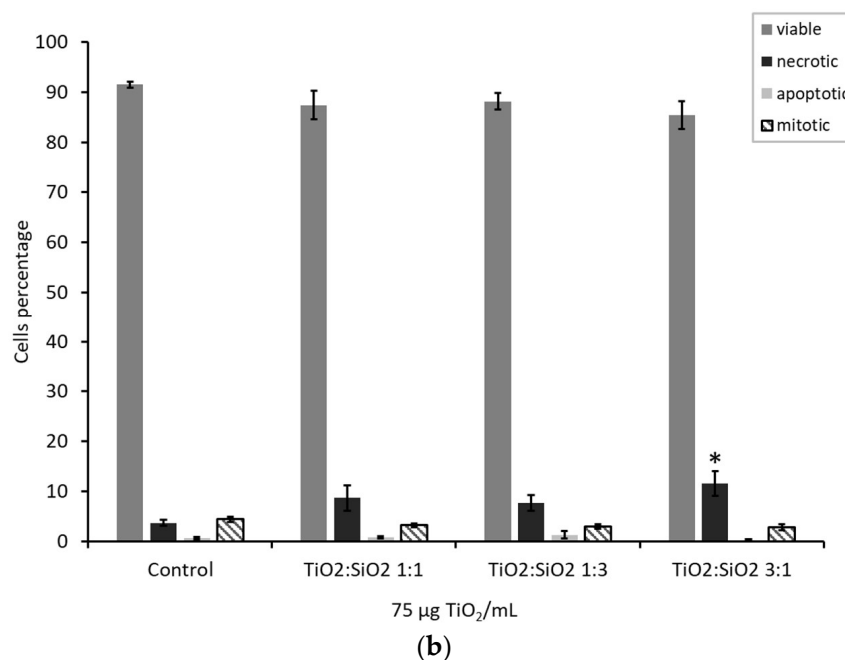


**Figure 4.** (a) Cell viability was assessed by MTT test after 24 h of exposure to increasing doses of different TiO<sub>2</sub>:SiO<sub>2</sub> NPs. The white histogram represents control sample, dark grey bars represent dose 750 µg TiO<sub>2</sub>/mL, grey bar dose 75 µg TiO<sub>2</sub>/mL, and light grey bars dose 7.5 µg TiO<sub>2</sub>/mL. Data show the mean ± SE of at least three independent experiments. \* Statistically significant with respect to control,  $p < 0.001$ ; # Statistically different with respect to TiO<sub>2</sub>:SiO<sub>2</sub> 1:1 at dose 750 µg TiO<sub>2</sub>/mL,  $p < 0.001$ ; § Statistically different with respect to TiO<sub>2</sub>:SiO<sub>2</sub> 1:3 at dose 750 µg TiO<sub>2</sub>/mL,  $p = 0.006$ . One-way ANOVA + Bonferroni's post hoc test. (b) Hoechst 33342/propidium iodide (H/PI) staining of A549 treated for 24 h with different TiO<sub>2</sub>:SiO<sub>2</sub> NPs (75 µg TiO<sub>2</sub>/mL). The histograms represent the percentage of viable (grey bars), necrotic (black bars), apoptotic (light grey bars), and mitotic (dashed bars) cells. Data show the mean ± SE of at least three independent experiments. \* Statistically significant with respect to control according to one-way ANOVA + Bonferroni's post hoc test;  $p < 0.05$ .

Data were also confirmed by the Annexin V/PI test, which evidenced that the exposure to TiO<sub>2</sub>:SiO<sub>2</sub> 3:1, as well as TiO<sub>2</sub> NPs alone, increased the percentage of early necrotic cells (Annexin V+/PI+). Thanks to the Annexin V test, a slight increase of apoptotic (Annexin V+) cells, after exposure to TiO<sub>2</sub>:SiO<sub>2</sub> 1:1, 3:1, and TiO<sub>2</sub> NPs alone, was appreciated (Supplementary Materials S3b,c).

### 3.2.2. Oxidative stress: Reactive Oxygen Species (ROS) Formation

The induction of oxidative stress was evaluated by measuring the intracellular levels of ROS at early time points (180 min). Data showed that only TiO<sub>2</sub>:SiO<sub>2</sub> 3:1 NPs at the dose of 75 µg/mL was able to induce a significant increase of ROS levels (3.5-fold) with respect to control (Figure 5). Data on TiO<sub>2</sub> and SiO<sub>2</sub> NPs alone are reported in the Supplementary Materials (Figure S4).

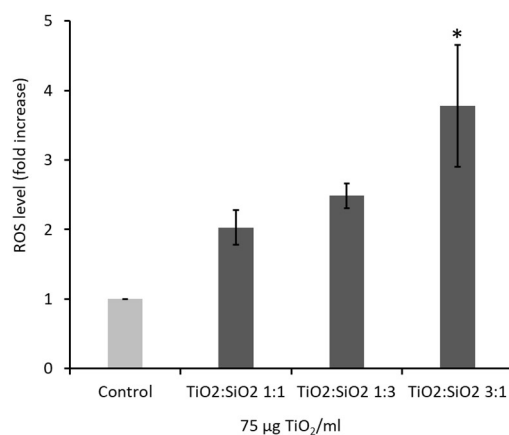


**Figure 5.** Oxidative stress was evaluated by detecting ROS in A549 after 180 min of exposure to TiO<sub>2</sub>:SiO<sub>2</sub> NPs (75 µg TiO<sub>2</sub>/mL) by using the fluorescent probe DCFDA. The histograms represent the mean ± SE of at least three independent experiments. \* Statistically significant with respect to control; One-way ANOVA + Bonferroni's post hoc test;  $p < 0.05$ .

### 3.2.3. Cell Cycle Analysis

The analysis of the cell cycle allows us to understand the potential of NPs to induce DNA damage. Data showed that TiO<sub>2</sub>:SiO<sub>2</sub> 3:1 NPs at the dose of 75 µg/mL induced a slight but significant arrest of the cell cycle in the S-phase (Figure 6). In fact, in control sample, 15.6% of cells were in the S-phase, while this percentage of cells is increased to 19.3% when treated with TiO<sub>2</sub>:SiO<sub>2</sub> 3:1 NPs.

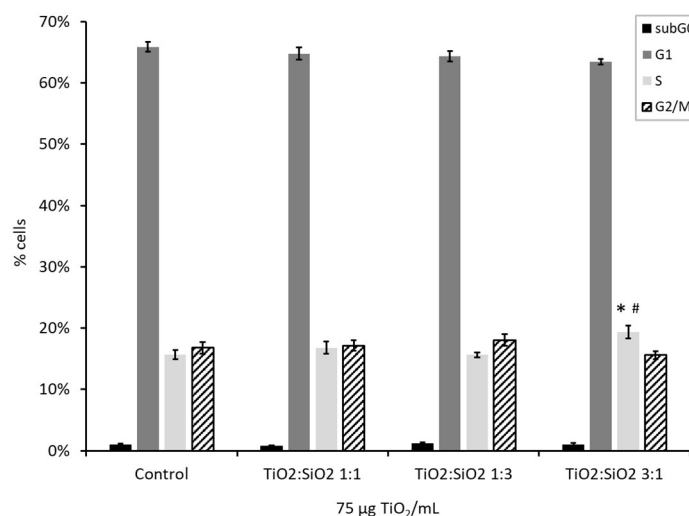


**Figure 6.** Different phases of the cell cycle (subG0, G1, S, and G2/M) were evaluated through Propidium Iodide content by cytofluorimetric analysis. The histograms represent the mean ± SE of at least three independent experiments. \* Statistically significant with respect to control sample; # Statistically significant with respect to the sample TiO<sub>2</sub>:SiO<sub>2</sub> 1:3. Unpaired *t*-test,  $p < 0.05$ .

### 3.2.4. NPs Induced Autophagy: LC3B II Expression

The analysis of the LC3BII protein allows us to understand the potential of NPs to induce cell autophagy. Data showed that TiO<sub>2</sub>:SiO<sub>2</sub> 1:1 and 3:1 NPs at the dose of 75 µg/mL induced a significant increase of LC3BII expression, while 1:3 NPs values are similar to the control one (Figure 7). Data on TiO<sub>2</sub> and SiO<sub>2</sub> NPs alone are reported in the Supplementary Materials (Figure S5).

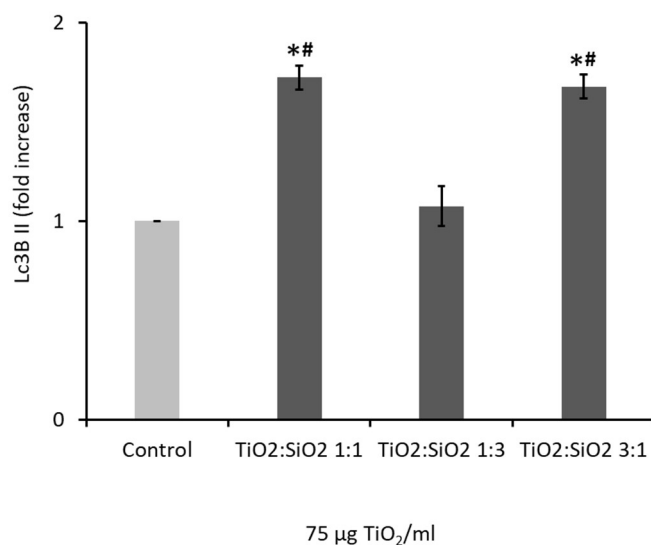


**Figure 7.** Autophagy was investigated through the analysis of the expression of LC3B II protein by cytofluorimeter. Cells were stained with LC3B II antibody after 24 h exposure to TiO<sub>2</sub>:SiO<sub>2</sub> NPs (75 µg TiO<sub>2</sub>/mL). The histograms represent the fold change of LC3B II expression over control, and they are the mean ± SE of at least three independent experiments. \* Statistically significant with respect to control; # Statistically different from sample TiO<sub>2</sub>:SiO<sub>2</sub> 1:3; *t*-test + Bonferroni's post hoc test; *p* < 0.05.

### 3.3. Cell Morphology and NPs Interaction

#### 3.3.1. Morphological Analysis

Data from HE staining showed that the exposure to the different NPs does not induce any significant morphological change (Figure 8). High magnification images (HM) clearly show the interaction of TiO<sub>2</sub>:SiO<sub>2</sub> NPs 1:1 and 3:1 with A549 cells, while an analog localization of NPs is not detectable in the cells exposed to TiO<sub>2</sub>:SiO<sub>2</sub> 1:3. On the contrary, high dimension aggregates are visible on these cells. Data on TiO<sub>2</sub> NPs alone are reported in the Supplementary Materials (Figure S6).

Furthermore, data from rhodamine phalloidin staining showed that the exposure to the different NPs seems to induce actin network morphological change (Figure 9). The interaction of TiO<sub>2</sub>:SiO<sub>2</sub> NPs 1:1 (Figure 9b) and 3:1 (Figure 9d) with A549 cells, increased cytoskeleton disassembly and the presence of cellular filopodia, while an analog localization of actin is not detectable in the cells exposed to TiO<sub>2</sub>:SiO<sub>2</sub> 1:3 (Figure 9c). Data on TiO<sub>2</sub> NPs alone are reported in the Supplementary Materials (Figure S7).

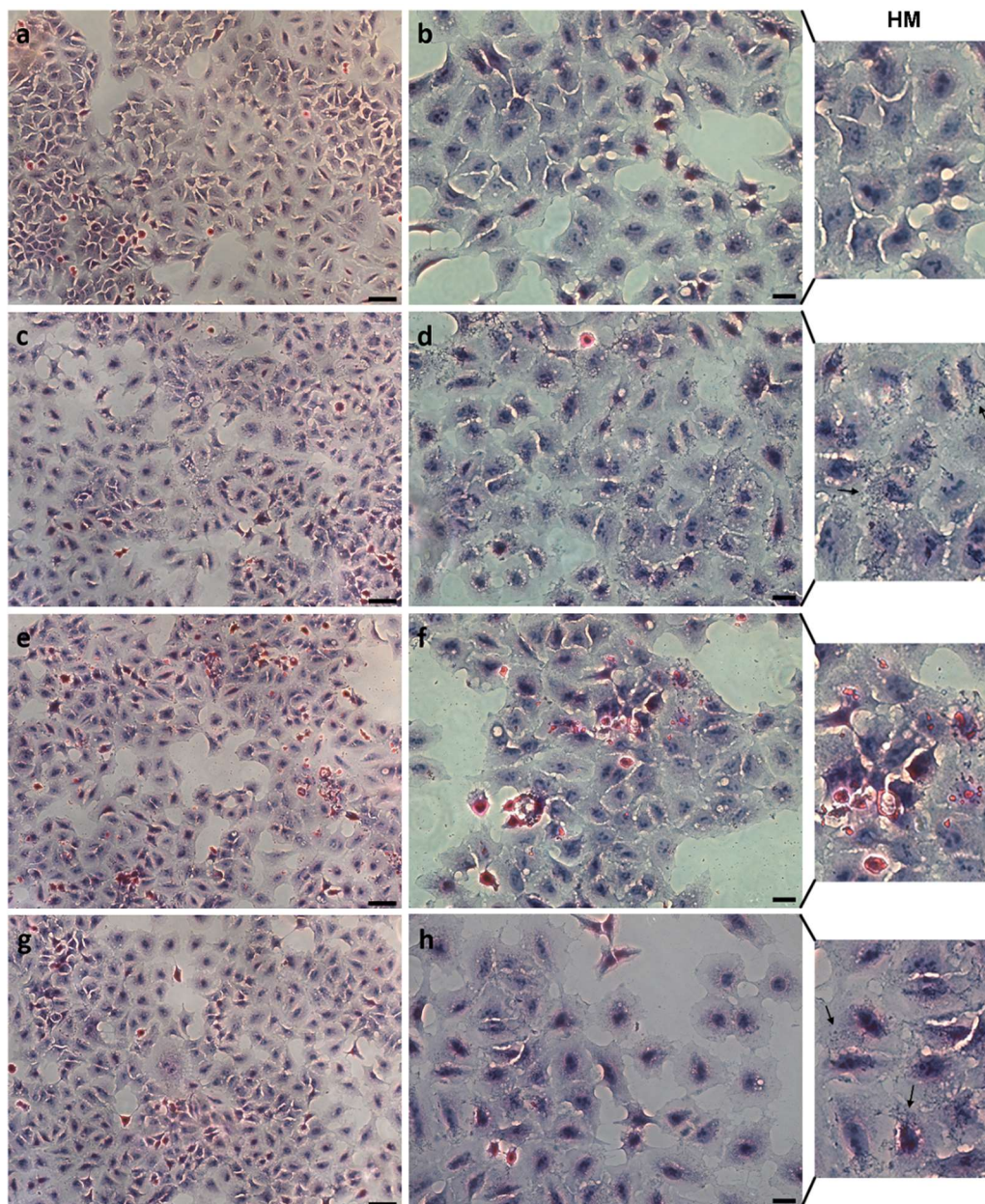


**Figure 8.** Morphology of cells after exposure to  $75 \mu\text{g TiO}_2/\text{mL}$  of  $\text{TiO}_2:\text{SiO}_2$  NPs 1:1 (c,d), 1:3 (e,f), 3:1 (g,h). Control cells are shown in (a,b). Cells were fixed and stained with Hematoxylin/Eosin. Scale bars:  $50 \mu\text{m}$  (a,c,e,g);  $20 \mu\text{m}$  (b,d,f,h). HM: high magnification of (b,d,f,h). Black arrows: nanoparticles interacting with cells.

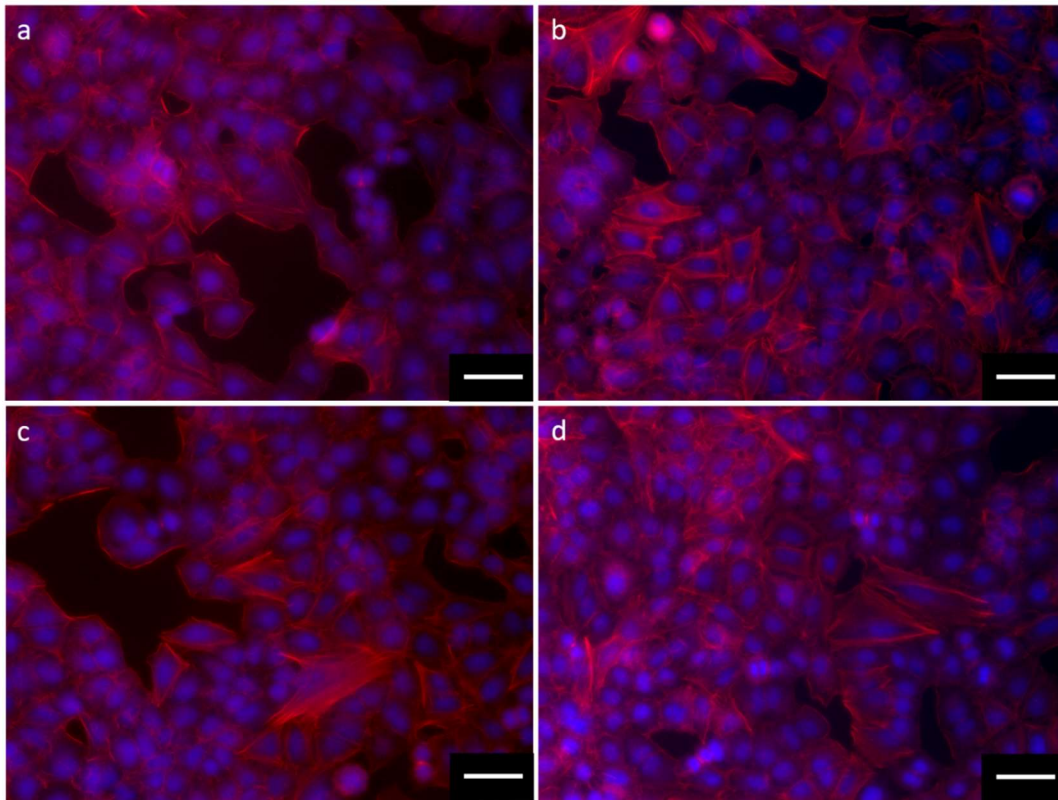


**Figure 9.** Morphology of cells after exposure to 75 µg TiO<sub>2</sub>/mL of TiO<sub>2</sub>:SiO<sub>2</sub> NPs 1:1 (**b**), 1:3 (**c**), 3:1 (**d**). Control cells are shown in (**a**). Cells were fixed and stained with DAPI (blue) and Rhodamine Phalloidin (red). Scale bars: 50 µm.

### 3.3.2. Cell–NP Interactions

The interaction among cells and NPs was investigated by analyzing the side scatter (SSC) of cells through cytofluorimetric analysis. Data showed that there is an increase of 1.3-fold in the SSC with TiO<sub>2</sub>:SiO<sub>2</sub> 1:1 and 3:1 NPs (Figure 10). This result confirms the higher interaction with A549 cells of TiO<sub>2</sub>:SiO<sub>2</sub> 1:1 and 3:1 NPs, as suggested by optical microscopy images, in line with the smaller size and more positive surface charge of these nanocomposites with respect to TiO<sub>2</sub>:SiO<sub>2</sub> 1:3 (Table 1). Data on TiO<sub>2</sub> NPs alone are reported in the Supplementary Materials (Figure S8).

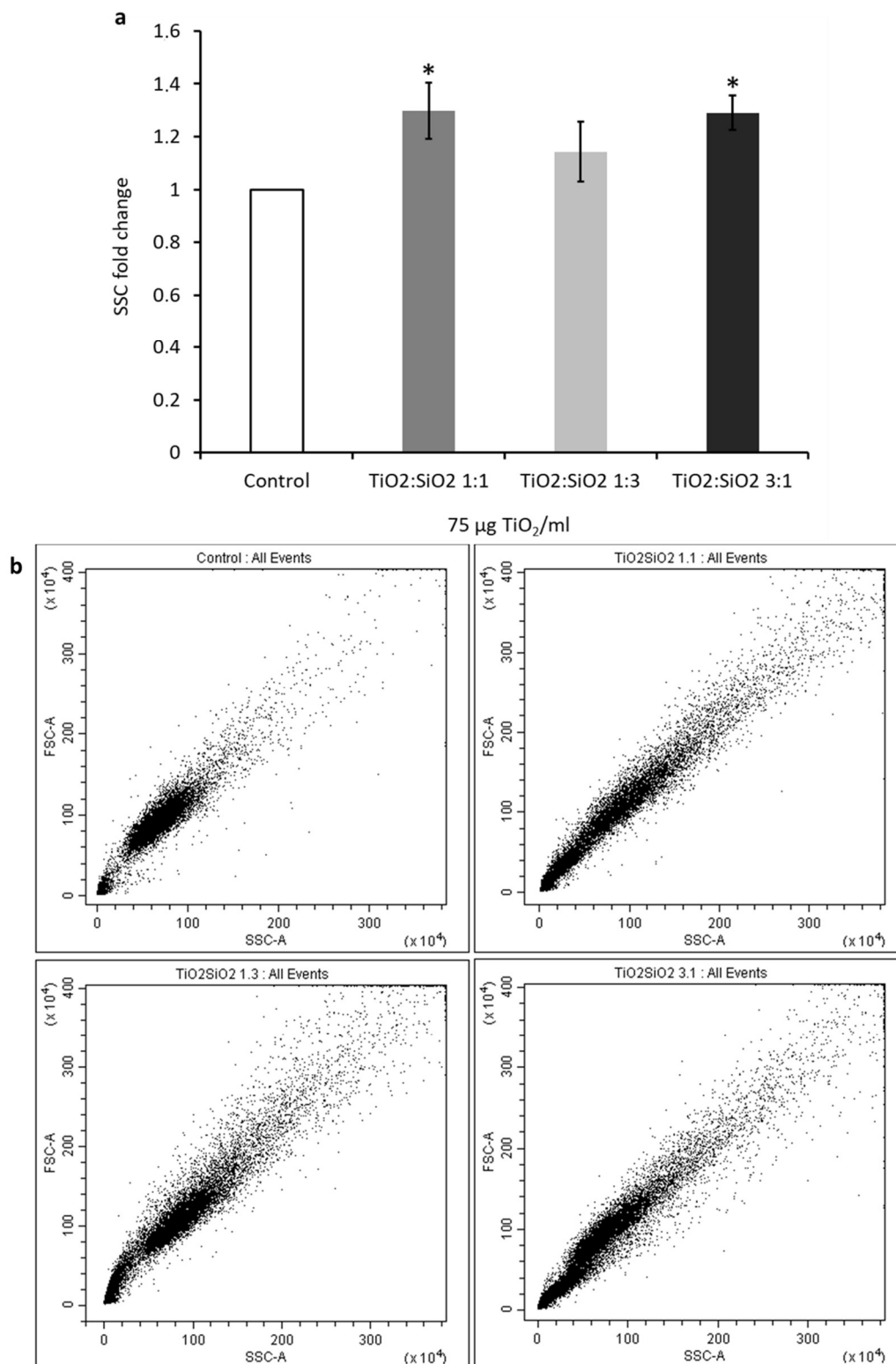


**Figure 10.** Cell and NP interactions after exposure for 24 h to TiO<sub>2</sub>:SiO<sub>2</sub> NPs. **(a)** The histograms show the fold change of side scatter (SSC), and data represent the mean ± SE of at least three independent experiments. **(b)** Representative dot-plots of forward scatter (FCS, *y*-axis) and side scatter (SSC, *x*-axis) of untreated cells (Control) and cells exposed for 24 h with TiO<sub>2</sub>:SiO<sub>2</sub> 1:1 (1.1), 1:3 (1.3), and 3:1 (3.1) NPs. \* Statistically significant with respect to control sample; unpaired *t*-test; *p* < 0.05.

#### 4. Discussion

Crystalline TiO<sub>2</sub> recently has gained great attention thanks to its special role in a wide range of applications in areas of photovoltaics, photocatalysis, photochromics, and sensors [33]. The employment of TiO<sub>2</sub> in industry has been a reality for almost 20 years [34], and TiO<sub>2</sub>-based nanomaterials are currently applied in a wide range of manufacturing fields (i.e., personal care, inks, plastics, food products, textiles, and medical devices) [35] and in the development of new anticancer therapies [36,37].

Materials coated with TiO<sub>2</sub> have long been described for their anti-bacterial properties [38]. Furthermore, TiO<sub>2</sub> nanotube coated surfaces can enhance osteoblast adhesion and proliferation [39]. Data on murine osteogenic cells demonstrated that the TiO<sub>2</sub> nanotube arrays can reduce *Staphylococcus epidermidis* colonization and enhance C3H10T1/2 cell adhesion and this dual effect is due to the multiple physical and chemical properties of the TiO<sub>2</sub> nanotube surface [40]. In 2016, Hashizume et al. demonstrated that after TiO<sub>2</sub> exposure alteration of the pulmonary inflammatory response may occur and may depend on the surface coating material. Therefore, the pulmonary toxicities of coated TiO<sub>2</sub> need to be further evaluated, and the physicochemical properties may be useful for predicting the pulmonary risk posed by new nano-TiO<sub>2</sub> materials [41].

It is likely that the use of TiO<sub>2</sub> and titania-based nanoparticles as antimicrobial devices is still limited by possible adverse effect on human health, especially upon the skin and pulmonary exposure [42]. Inhalation of engineered NPs, including TiO<sub>2</sub> NPs, mainly occurs during their production and use in laboratories, industries, and factories, but it is important to consider the whole nanomaterial lifecycle from the perspective of possible releases into the environment. TiO<sub>2</sub> NPs have been widely investigated for their cytotoxic effects, mainly due to their capability to induce oxidative stress under UV-irradiation [9], but also when not photoactivated [11–13]. A recent study has reported how airborne TiO<sub>2</sub> NPs can induce oxidative stress under outdoor conditions, including UV-irradiation and relative humidity [43], corroborating the crucial issue of TiO<sub>2</sub> NPs risk assessment, due to the widespread distribution of nanomaterials in the environment [44,45].

In the last decade, different TiO<sub>2</sub>:SiO<sub>2</sub> nanostructures were designed to enhance TiO<sub>2</sub> photocatalytic effect [8,46], but TiO<sub>2</sub> encapsulation in SiO<sub>2</sub> matrix was also demonstrated effective in reducing ROS production. The protective role of SiO<sub>2</sub> on TiO<sub>2</sub>-induced oxidative stress was demonstrated by spectroscopic quantification of free radicals production by spin trap molecules [14], suggesting a promising safety outcome in live cells.

In the current study, a comparison of cytotoxicity of TiO<sub>2</sub>:SiO<sub>2</sub> NPs having different ratios of TiO<sub>2</sub> and SiO<sub>2</sub> was performed by analyzing their effects on A549 viability, cell cycle, morphology, and oxidative stress. Cells viability was first assessed after exposure to TiO<sub>2</sub>:SiO<sub>2</sub> 1:1, TiO<sub>2</sub>:SiO<sub>2</sub> 1:3, and TiO<sub>2</sub>:SiO<sub>2</sub> 3:1 with an NP concentration ranging from 7.5 to 750 µg TiO<sub>2</sub>/mL, which is representative of realistic human exposure [47].

A significant impact on cell viability was observed only with TiO<sub>2</sub>:SiO<sub>2</sub> 3:1 at the higher concentrations and necrosis, and slight apoptosis, seems to be the main pathways of cell death. A549 necrosis induced by exposure to 75 µg TiO<sub>2</sub>/mL TiO<sub>2</sub>:SiO<sub>2</sub> 3:1 is mediated by increasing reactive oxygen species, according to mechanisms widely described in literature concerning NPs cytotoxicity [48,49].

The comparison with the biological effects induced by the exposure TiO<sub>2</sub> and SiO<sub>2</sub> NPs alone is quite controversial, but to have a complete overview of the differences between diverse NMs properties, several endpoints have also been investigated after TiO<sub>2</sub> and SiO<sub>2</sub> treatment.

In particular, cytotoxicity was investigated for both SiO<sub>2</sub> and TiO<sub>2</sub> NPs alone and data revealed that SiO<sub>2</sub> NPs are highly toxic even at the intermediate dose of exposure, while TiO<sub>2</sub> induced cell reduction only at the dose of 750 µg/mL. Compared to cytotoxicity TiO<sub>2</sub> NPs values, TiO<sub>2</sub>:SiO<sub>2</sub> 3:1 NPs resulted more toxic. These could be explained by the fact that the nanocomposites are physically different from TiO<sub>2</sub> and SiO<sub>2</sub> single NPs nanoparticles. This evidence is confirmed by TEM and DLS results and from previous data from Ortelli et al. [8], in which authors have demonstrated that in an aqueous medium TiO<sub>2</sub>/SiO<sub>2</sub> samples have a different behavior/reactivity towards water compared to

titania and silica alone. The presence of SiO<sub>2</sub> in the TiO<sub>2</sub> matrix increased the number of adsorbed molecules without modifying adsorption energy. The addition of SiO<sub>2</sub> caused an increase in the surface hydrophilicity of titania. Even if the TiO<sub>2</sub> NPs used in these works are not highly cytotoxic, there are evidences of induced biological effects, such as necrosis, autophagy, ROS induction, and morphological changes (Supplementary Materials). Furthermore, SiO<sub>2</sub> NPs, which have a very low size (20 nm), are even more toxic of TiO<sub>2</sub> NPs alone and TiO<sub>2</sub>:SiO<sub>2</sub> NPs. Nevertheless, TiO<sub>2</sub> and SiO<sub>2</sub> NPs alone are not good photocatalysts, and for these reasons, these NPs were combined to improve TiO<sub>2</sub> effectiveness in a safe manner.

The lack of any significant effect of colloidal TiO<sub>2</sub>:SiO<sub>2</sub> 1:3 NPs on the oxidative state of living A549 cells is in line with previous results obtained by Ortelli et al. using a comparable concentration of NPs for a longer exposure time [24]. Moreover, differently from the previous work of Ortelli and colleagues, in the present work, the effect on cells viability, cells cycle, and cell–NP interaction was investigated and nanocomposites with different of TiO<sub>2</sub>:SiO<sub>2</sub> ratio compared, pointing out that the modification of physicochemical properties, by safe-by-design approach, is crucial in estimating potential *in vitro* biological responses [50].

Data about the cytotoxic effects of silica-coated-TiO<sub>2</sub> are in line with *in vivo* findings on mice, in which these NMs induced pulmonary and sensory irritation after single and repeated exposure and airflow limitation and pulmonary inflammation after repeated exposure [51].

DNA damage is one of the major effects of ROS production [52], and analysis of cell cycle phases is a fast screening for the evaluation of possible alteration at the DNA level after exposure to NPs. Alteration of the cell cycle is, therefore, a marker of genotoxicity. We observed that TiO<sub>2</sub>:SiO<sub>2</sub> 3:1 was able to induce a slight but significant arrest of the cell cycle in the S-phase. Previous data have reported that TiO<sub>2</sub> NPs cause arrest in the G2/M-phase [53], even if other evidences have reported a TiO<sub>2</sub> NPs-induced G1/S-phase arrest due the presence of DNA strand breaks as a consequence of oxidative stress. The arrest in the G1/S and S-phase has also been previously demonstrated in response to other nanoparticles (e.g., ZnO or AuNPs) and with different cell targets [54].

In 2015, Wang et al. demonstrated that TiO<sub>2</sub> NPs can inhibit A549 cell proliferation, cause DNA damage, and induce apoptosis via a mechanism primarily involving the activation of the intrinsic mitochondrial pathway, suggesting that exposure to TiO<sub>2</sub> NPs could cause cell injury and be hazardous to health [55]. Furthermore, *in vivo* experiments showed that exposure in mice to different ratios of SiO<sub>2</sub>:TiO<sub>2</sub> NPs, induced different effects on DNA damage evidencing that SiO<sub>2</sub>:TiO<sub>2</sub> composite induced *in vivo* toxicity, oxidative DNA damage, bargain of the antioxidant enzymes, while SiO<sub>2</sub>:ZrO<sub>2</sub> composites revealed a lower toxicity in mice compared with that of TiO<sub>2</sub> [56]. These results confirmed that TiO<sub>2</sub> NPs can potentially cause adverse effects on organ, tissue, cellular, subcellular, and protein levels due to their unusual physicochemical properties [57].

Another molecular mechanism activated by metal oxide NPs exposure, including titanium dioxide TiO<sub>2</sub> NPs, is the autophagic pathway associated with toxic effects [38,58,59]. Dysfunction in autophagy could be due to the metal oxide NPs' ability to increase oxidative stress and cationic damage. Autophagy is an evolutionarily conserved cellular quality control process, and in the case of toxicant and/or metal-induced toxicity, autophagy may act as a survival mechanism by targeting novice components to the lysosomes for degradation [60]. However, excess autophagy may also lead to cell death. Lopes and colleagues [61] showed that the uptake of TiO<sub>2</sub> NPs leads to a dose-dependent increase in autophagic effect under non-cytotoxic conditions as a cellular response to TiO<sub>2</sub> NPs and they suggested that simple toxicity data are not enough to understand the full impact of TiO NPs and their effects on cellular pathways or function.

Microtubule-associated protein light-chain protein-3 (LC3) is a key protein in autophagosome formation, and it is converted from its cytosolic form (LC3 I) into an active membrane-bound form (LC3 II) by sequential proteolysis and lipidation during autophagosome assembly [54]. Our data on LC3B II expression confirm that autophagy occurs with TiO<sub>2</sub>:SiO<sub>2</sub> 1:1, 3:1, and TiO<sub>2</sub> NPs, confirming that autophagy is one of the main pathways involved in the response to metal oxide NPs.

Therefore, while TiO<sub>2</sub>:SiO<sub>2</sub> 1:1 and TiO<sub>2</sub>:SiO<sub>2</sub> 1:3 are totally ineffective on A549, TiO<sub>2</sub>:SiO<sub>2</sub> 3:1 is able to exert a cytotoxic effect, based on ROS-dependent necrosis, autophagy, and cell cycle arrest.

Although TiO<sub>2</sub> NPs exposure can induce limited cytotoxicity, they can affect/disassembly actin and tubulin networks with consequent alterations in the cytoskeleton. In addition, proteomic analyses have evidenced that some alterations in proteins related to cytoskeleton disturbances may occur after TiO<sub>2</sub> NPs exposure [62].

No significant alterations have been observed in the morphology of cells exposed to the three types of silica-modified TiO<sub>2</sub> nano formulation with hematoxylin and eosin (HE/E) staining. Nevertheless, high magnification images show that the interaction between cells and TiO<sub>2</sub>:SiO<sub>2</sub> 1:1 and 3:1 are more similar to each other and to TiO<sub>2</sub> NPs compared to NPs 1:3, as also shown by side scattering analyses. Moreover, further investigations on the actin microfilaments showed that the exposure to TiO<sub>2</sub>:SiO<sub>2</sub> 1:1, 3:1, and TiO<sub>2</sub> induced modification of cellular cytoskeleton. In particular, the increased localization of actin protein at the cellular cortex, loss of stress fibers, and increased filopodia could be due to the more evident interaction between cells and NPs.

Cytoskeleton alterations may be related to oxidative stress and inflammation even under low concentrations of NP exposure, as well as direct effects on cytoskeleton components.

The different distribution of NPs within A549 cells is in line with their physicochemical parameters: TiO<sub>2</sub>:SiO<sub>2</sub> 1:1 and 3:1 have dimensions in the nanometric range (126 and 148 nm, respectively), highly positive surface charge and low polydispersity index are favorable to efficient interaction with cells. The lower positive  $\zeta$ -potential and the higher PDI of TiO<sub>2</sub>:SiO<sub>2</sub> 1:3 indicates that these NPs are less stable in water suspension and tend to form big agglomerates, as also proved by the large hydrodynamic size and confirmed by microscopy observation.

Previous works have reported that the silica coating reduces the toxic effects of other antimicrobial NPs, such as zinc oxide (ZnO) and iron oxide (Fe<sub>3</sub>O<sub>4</sub>) nanoparticles [17,18]. Silica prevents zinc and iron toxicity because it improves their stability in the biological fluids, reducing oxidative stress and their overall cytotoxicity and genotoxicity. Moreover, bare NPs release more zinc and iron ions in the intracellular space, with a stronger in situ degradation. In our case, encapsulation is likely not working by preventing ions dissolution from the NP surface, even considering that TiO<sub>2</sub> is poorly solubilized in an aqueous cellular medium [63]. It is more likely that SiO<sub>2</sub> encapsulation is able to mask the titania crystal surface, which in turn may produce local ROS once in contact with intracellular molecules.

## 5. Conclusions

In recent studies, SiO<sub>2</sub>-modified TiO<sub>2</sub> NPs have been proposed as photocatalytic and anti-bacterial devices for surface coatings of different materials (e.g., textiles). Silica coating increases the photocatalytic activity of titania NPs and at the same time reduces the potential toxic effects induced by TiO<sub>2</sub>. The current application of photoactive TiO<sub>2</sub> nanoparticles in many industrial fields raises the crucial issue of their safety both for workers, in the production sites, and end-users. In this scenario, our study not only confirms the relevance of silica coating as a powerful strategy to prevent the adverse impact of TiO<sub>2</sub> NPs but also provides an exact indication on the most effective SiO<sub>2</sub> vs. TiO<sub>2</sub> ratio into the nanocomposite. Higher protection is obtained in recent studies. SiO<sub>2</sub>-modified TiO<sub>2</sub> NPs have been proposed as photocatalytic and anti-bacterial devices for surface coatings of different materials (e.g., textiles). Silica coating increases the photocatalytic activity of titania NPs and at the same time, reduces the potential toxic effects induced by TiO<sub>2</sub>. The major toxic effects induced by TiO<sub>2</sub> are triggered by oxidative stress, which leads to cellular necrosis and DNA damage. The size and physical properties of NPs are partly responsible for the NPs toxicity, with particles with smaller size and higher stability are more interactive with pulmonary cells. The encapsulation of TiO<sub>2</sub> NPs in a SiO<sub>2</sub> matrix with the higher content of SiO<sub>2</sub> vs. TiO<sub>2</sub> decreases the cytotoxic effects of TiO<sub>2</sub>.

The major toxic effects induced by TiO<sub>2</sub> are triggered by oxidative stress, which leads to cellular necrosis and DNA damage. The size and physical properties of NPs are partly responsible for the NPs

toxicity, with particles with smaller size and higher stability being more interactive with pulmonary cells. The chemical composition of NPs and the ratio among silica and titania plays a crucial role in the induction of the observed biological effects posing great attention in the design of these nanomaterials for their safe application in several industrial and research fields.

**Supplementary Materials:** The following are available online at <http://www.mdpi.com/2079-4991/9/7/1041/s1>, Figure S1: TEM images of a) TiO<sub>2</sub> and b) SiO<sub>2</sub> nanoparticles. Figure S2: Cell viability was assessed by MTT test after 24h of exposure to increasing doses of TiO<sub>2</sub> (dark grey bars) and SiO<sub>2</sub> (grey bars) NPs. Figure S3: Hoechst/PI test and Annexin V/PI assay for the evaluation of necrotic and apoptotic cells. Figure S4: Oxidative stress was evaluating by detecting ROS in A549 after 180 min of exposure to TiO<sub>2</sub> and SiO<sub>2</sub> NPs (75 µg/mL) and positive control H<sub>2</sub>O<sub>2</sub> (100 µM) by using the fluorescent probe DCFDA. Figure S5: Autophagy was investigated through the analysis of the expression of LC3B II protein by cytofluorimeter. Figure S6: Morphology of cells after exposure to 75 µg/mL of TiO<sub>2</sub>. Figure S7: Morphology of cells after exposure to 75 µg/mL of TiO<sub>2</sub>. Figure S8: Cells and NPs interactions after exposure for 24h to TiO<sub>2</sub> NPs.

**Author Contributions:** Conceptualization, P.M. and L.F.; Methodology, R.B. and S.O.; Investigation, R.B. and S.O.; Data Curation, R.B. and S.O.; Writing—Original Draft Preparation, R.B. and L.F.; Writing—Review and Editing, R.B., S.O., M.B., A.C., P.M., and L.F.; Supervision, L.F. and P.M.; Funding Acquisition, P.M.

**Funding:** This work was funded by the European Community's Horizon 2020 Framework Program H2020 (H2020-720851 project PROTECT—Pre-commercial lines for production of surface nanostructured antimicrobial and anti-biofilm textiles, medical devices, and water treatment membranes) ([www.protect-h2020.eu](http://www.protect-h2020.eu)).

**Conflicts of Interest:** The authors declare no conflict of interest.

## References

- Hajipour, M.J.; Fromm, K.M.; Akbar Ashkarran, A.; Jimenez de Aberasturi, D.; de Larramendi, I.R.; Rojo, T.; Serpooshan, V.; Parak, W.J.; Mahmoudi, M. Antibacterial properties of nanoparticles. *Trends Biotechnol.* **2012**, *30*, 499–511. [[CrossRef](#)] [[PubMed](#)]
- Jin, S.-E.; Jin, J.E.; Hwang, W.; Hong, S.W. Photocatalytic antibacterial application of zinc oxide nanoparticles and self-assembled networks under dual UV irradiation for enhanced disinfection. *Int. J. Nanomed.* **2019**, *14*, 1737–1751. [[CrossRef](#)] [[PubMed](#)]
- Thevenot, P.; Cho, J.; Wavhal, D.; Timmons, R.B.; Tang, L. Surface chemistry influences cancer killing effect of TiO<sub>2</sub> nanoparticles. *Nanomedicine* **2008**, *4*, 226–236. [[CrossRef](#)] [[PubMed](#)]
- Bogdan, J.; Pławińska-Czarnak, J.; Zarzyńska, J. Nanoparticles of Titanium and Zinc Oxides as Novel Agents in Tumor Treatment: A Review. *Nanoscale Res. Lett.* **2017**, *12*, 225. [[CrossRef](#)] [[PubMed](#)]
- Matsunaga, T.; Tomoda, R.; Nakajima, T.; Wake, H. Photoelectrochemical sterilization of microbial cells by semiconductor powders. *FEMS Microbiol. Lett.* **1985**, *29*, 211–214. [[CrossRef](#)]
- Nakata, K.; Fujishima, A. TiO<sub>2</sub> photocatalysis: Design and applications. *J. Photochem. Photobiol. C Photochem. Rev.* **2012**, *13*, 169–189. [[CrossRef](#)]
- Luttrell, T.; Halpegamage, S.; Tao, J.; Kramer, A.; Sutter, E.; Batzill, M. Why is anatase a better photocatalyst than rutile?—Model studies on epitaxial TiO<sub>2</sub> films. *Sci. Rep.* **2015**, *4*, 4043. [[CrossRef](#)]
- Ortelli, S.; Blosi, M.; Delpivo, C.; Gardini, D.; Dondi, M.; Gualandi, I.; Tonelli, D.; Aina, V.; Fenoglio, I.; Gandhi, A.A.; et al. Multiple approach to test nano TiO<sub>2</sub> photo-activity. *J. Photochem. Photobiol. A Chem.* **2014**, *292*, 26–33. [[CrossRef](#)]
- Yin, J.-J.; Liu, J.; Ehrenshaft, M.; Roberts, J.E.; Fu, P.P.; Mason, R.P.; Zhao, B. Phototoxicity of nano titanium dioxides in HaCaT keratinocytes—Generation of reactive oxygen species and cell damage. *Toxicol. Appl. Pharmacol.* **2012**, *263*, 81–88. [[CrossRef](#)]
- Sun, J.; Guo, L.-H.; Zhang, H.; Zhao, L. UV Irradiation Induced Transformation of TiO<sub>2</sub> Nanoparticles in Water: Aggregation and Photoreactivity. *Environ. Sci. Technol.* **2014**, *48*, 11962–11968. [[CrossRef](#)]
- Huerta-García, E.; Pérez-Arizti, J.A.; Márquez-Ramírez, S.G.; Delgado-Buenrostro, N.L.; Chirino, Y.I.; Iglesias, G.G.; López-Marure, R. Titanium dioxide nanoparticles induce strong oxidative stress and mitochondrial damage in glial cells. *Free Radic. Biol. Med.* **2014**, *73*, 84–94. [[CrossRef](#)]
- Dubey, A.; Goswami, M.; Yadav, K.; Chaudhary, D. Oxidative Stress and Nano-Toxicity Induced by TiO<sub>2</sub> and ZnO on WAG Cell Line. *PLoS ONE* **2015**, *10*, e0127493. [[CrossRef](#)]

13. Hanot-Roy, M.; Tubeuf, E.; Guilbert, A.; Bado-Nilles, A.; Vigneron, P.; Trouiller, B.; Braun, A.; Lacroix, G. Oxidative stress pathways involved in cytotoxicity and genotoxicity of titanium dioxide (TiO<sub>2</sub>) nanoparticles on cells constitutive of alveolo-capillary barrier in vitro. *Toxicol. Vitro* **2016**, *33*, 125–135. [[CrossRef](#)]
14. Ortelli, S.; Poland, C.A.; Baldi, G.; Costa, A.L. Silica matrix encapsulation as a strategy to control ROS production while preserving photoreactivity in nano-TiO<sub>2</sub>. *Environ. Sci. Nano* **2016**, *3*, 602–610. [[CrossRef](#)]
15. Gawande, M.B.; Goswami, A.; Asefa, T.; Guo, H.; Biradar, A.V.; Peng, D.-L.; Zboril, R.; Varma, R.S. Core-shell nanoparticles: Synthesis and applications in catalysis and electrocatalysis. *Chem. Soc. Rev.* **2015**, *44*, 7540–7590. [[CrossRef](#)]
16. Ivanova, A.; Ivanova, K.; Hoyo, J.; Heinze, T.; Sanchez-Gomez, S.; Tzanov, T. Layer-By-Layer Decorated Nanoparticles with Tunable Antibacterial and Antibiofilm Properties against Both Gram-Positive and Gram-Negative Bacteria. *ACS Appl. Mater. Interface* **2018**, *10*, 3314–3323. [[CrossRef](#)]
17. Chia, S.L.; Leong, D.T. Reducing ZnO nanoparticles toxicity through silica coating. *Heliyon* **2016**, *2*, e00177. [[CrossRef](#)]
18. Malvindi, M.A.; De Matteis, V.; Galeone, A.; Brunetti, V.; Anyfantis, G.C.; Athanassiou, A.; Cingolani, R.; Pompa, P.P. Toxicity Assessment of Silica Coated Iron Oxide Nanoparticles and Biocompatibility Improvement by Surface Engineering. *PLoS ONE* **2014**, *9*, e85835. [[CrossRef](#)]
19. Ortelli, S.; Costa, A.L. Nanoencapsulation techniques as a “safer by (molecular) design” tool. *Nano-Struct. Nano-Objects* **2018**, *13*, 155–162. [[CrossRef](#)]
20. Srivastava, R.; Rahman, Q.; Kashyap, M.; Singh, A.; Jain, G.; Jahan, S.; Lohani, M.; Lantow, M.; Pant, A. Nano-titanium dioxide induces genotoxicity and apoptosis in human lung cancer cell line, A549. *Hum. Exp. Toxicol.* **2013**, *32*, 153–166. [[CrossRef](#)]
21. Fröhlich, E.; Salar-Behzadi, S. Toxicological Assessment of Inhaled Nanoparticles: Role of in Vivo, ex Vivo, in Vitro, and in Silico Studies. *Int. J. Mol. Sci.* **2014**, *15*, 4795–4822. [[CrossRef](#)]
22. Castell, J.V.; Donato, M.T.; Gómez-Lechón, M.J. Metabolism and bioactivation of toxicants in the lung. The in vitro cellular approach. *Exp. Toxicol. Pathol.* **2005**, *57* (Suppl. 1), 189–204. [[CrossRef](#)]
23. Van Teunenbroek, T. *NANOREG, a Common European Approach to the Regulatory Testing of Nanomaterials Final Report (Part 1)*; Ministry of Infrastructure and the Environment: The Hague, The Netherlands, 2016.
24. Ortelli, S.; Costa, A.L.; Matteucci, P.; Miller, M.R.; Blosi, M.; Gardini, D.; Tofail, S.A.M.; Tran, L.; Tonelli, D.; Poland, C.A. Silica modification of titania nanoparticles enhances photocatalytic production of reactive oxygen species without increasing toxicity potential in vitro. *RSC Adv.* **2018**, *8*, 40369–40377. [[CrossRef](#)]
25. Gualtieri, M.; Rigamonti, L.; Galeotti, V.; Camatini, M. Toxicity of tire debris extracts on human lung cell line A549. *Toxicol. Vitro* **2005**, *19*, 1001–1008. [[CrossRef](#)]
26. Mosmann, T. Rapid colorimetric assay for cellular growth and survival: Application to proliferation and cytotoxicity assays. *J. Immunol. Methods* **1983**, *65*, 55–63. [[CrossRef](#)]
27. Bengalli, R.; Zerboni, A.; Marchetti, S.; Longhin, E.; Priola, M.; Camatini, M.; Mantecca, P. In vitro pulmonary and vascular effects induced by different diesel exhaust particles. *Toxicol. Lett.* **2019**, *306*, 13–24. [[CrossRef](#)]
28. Zuidam, N.J.; Nedovic, V. *Encapsulation Technologies for Active Food Ingredients*; Springer: Berlin, Germany, 2012; ISBN 9781441910073.
29. Wu, Q.; Wang, Z.; Kong, X.; Gu, X.; Xue, G. A Facile Strategy for Controlling the Self-Assembly of Nanocomposite Particles Based on Colloidal Steric Stabilization Theory. *Langmuir* **2008**, *24*, 7778–7784. [[CrossRef](#)]
30. Sun, J.; Gao, L. Development of a dispersion process for carbon nanotubes in ceramic matrix by heterocoagulation. *Carbon* **2003**, *41*, 1063–1068. [[CrossRef](#)]
31. Drasler, B.; Sayre, P.; Steinhäuser, K.G.; Petri-Fink, A.; Rothen-Rutishauser, B. In vitro approaches to assess the hazard of nanomaterials. *Nano Impact* **2017**, *8*, 99–116. [[CrossRef](#)]
32. Farcas, L.; Torres Andón, F.; Di Cristo, L.; Rotoli, B.M.; Bussolati, O.; Bergamaschi, E.; Mech, A.; Hartmann, N.B.; Rasmussen, K.; Riego-Sintes, J.; et al. Comprehensive In Vitro Toxicity Testing of a Panel of Representative Oxide Nanomaterials: First Steps towards an Intelligent Testing Strategy. *PLoS ONE* **2015**, *10*, e0127174. [[CrossRef](#)]
33. Gupta, S.; Tripathi, M. A review on the synthesis of TiO<sub>2</sub> nanoparticles by solution route. *Open Chem.* **2012**, *10*, 279–294. [[CrossRef](#)]
34. Hashimoto, K.; Irie, H.; Fujishima, A. TiO<sub>2</sub> Photocatalysis: A Historical Overview and Future Prospects. *Jpn. J. Appl. Phys.* **2005**, *44*, 8269–8285. [[CrossRef](#)]

35. Waghmode, M.S.; Gunjal, A.B.; Mulla, J.A.; Patil, N.N.; Nawani, N.N. Studies on the titanium dioxide nanoparticles: Biosynthesis, applications and remediation. *SN Appl. Sci.* **2019**, *1*, 310. [[CrossRef](#)]
36. Çeşmeli, S.; Biray Avci, C. Application of titanium dioxide (TiO<sub>2</sub>) nanoparticles in cancer therapies. *J. Drug Target.* **2019**, *27*, 762–766. [[CrossRef](#)]
37. Oh, W.-K.; Kim, S.; Choi, M.; Kim, C.; Jeong, Y.S.; Cho, B.-R.; Hahn, J.-S.; Jang, J. Cellular Uptake, Cytotoxicity, and Innate Immune Response of Silica–Titania Hollow Nanoparticles Based on Size and Surface Functionality. *ACS Nano* **2010**, *4*, 5301–5313. [[CrossRef](#)]
38. Muranyi, P.; Schraml, C.; Wunderlich, J. Antimicrobial efficiency of titanium dioxide-coated surfaces. *J. Appl. Microbiol.* **2009**, *108*, 1966–1973. [[CrossRef](#)]
39. Eaninwene, G.; Yao, C.; Webster, T.J. Enhanced osteoblast adhesion to drug-coated anodized nanotubular titanium surfaces. *Int. J. Nanomed.* **2008**, *3*, 257–264.
40. Tang, T.; Peng, J.; Ni, K.; Zheng, Y.; Shen, X.; Wang, G.; He, S.; Jin, T. Dual effects and mechanism of TiO<sub>2</sub> nanotube arrays in reducing bacterial colonization and enhancing C3H10T1/2 cell adhesion. *Int. J. Nanomed.* **2013**, *8*, 3093. [[CrossRef](#)]
41. Hashizume, N.; Oshima, Y.; Nakai, M.; Kobayashi, T.; Sasaki, T.; Kawaguchi, K.; Honda, K.; Gamo, M.; Yamamoto, K.; Tsubokura, Y.; et al. Categorization of nano-structured titanium dioxide according to physicochemical characteristics and pulmonary toxicity. *Toxicol. Rep.* **2016**, *3*, 490–500. [[CrossRef](#)]
42. Shakeel, M.; Jabeen, F.; Shabbir, S.; Asghar, M.S.; Khan, M.S.; Chaudhry, A.S. Toxicity of Nano-Titanium Dioxide (TiO<sub>2</sub>-NP) Through Various Routes of Exposure: A Review. *Biol. Trace Elem. Res.* **2016**, *172*, 1–36. [[CrossRef](#)]
43. Vernez, D.; Sauvain, J.-J.; Laulagnet, A.; Otaño, A.P.; Hopf, N.B.; Batsungnoen, K.; Suárez, G. Airborne nano-TiO<sub>2</sub> particles: An innate or environmentally-induced toxicity? *J. Photochem. Photobiol. A Chem.* **2017**, *343*, 119–125. [[CrossRef](#)]
44. Shah, S.N.A.; Shah, Z.; Hussain, M.; Khan, M. Hazardous Effects of Titanium Dioxide Nanoparticles in Ecosystem. *Bioinorg. Chem. Appl.* **2017**, *2017*, 4101735. [[CrossRef](#)]
45. John, A.; Küpper, M.; Manders-Groot, A.; Debray, B.; Lacombe, J.-M.; Kuhlbusch, T.; John, A.C.; Küpper, M.; Manders-Groot, A.M.M.; Debray, B.; et al. Emissions and Possible Environmental Implication of Engineered Nanomaterials (ENMs) in the Atmosphere. *Atmosphere* **2017**, *8*, 84. [[CrossRef](#)]
46. Hu, S.; Li, F.; Fan, Z. Preparation of SiO<sub>2</sub>-Coated TiO<sub>2</sub> Composite Materials with Enhanced Photocatalytic Activity Under UV Light. *Bull. Korean Chem. Soc.* **2012**, *33*, 1895–1899. [[CrossRef](#)]
47. Gangwal, S.; Brown, J.S.; Wang, A.; Houck, K.A.; Dix, D.J.; Kavlock, R.J.; Hubal, E.A.C. Informing Selection of Nanomaterial Concentrations for ToxCast in Vitro Testing Based on Occupational Exposure Potential. *Environ. Health Perspect.* **2011**, *119*, 1539–1546. [[CrossRef](#)]
48. Abdal Dayem, A.; Hossain, M.K.; Lee, S.B.; Kim, K.; Saha, S.K.; Yang, G.-M.; Choi, H.Y.; Cho, S.-G. The Role of Reactive Oxygen Species (ROS) in the Biological Activities of Metallic Nanoparticles. *Int. J. Mol. Sci.* **2017**, *18*. [[CrossRef](#)]
49. Khanna, P.; Ong, C.; Bay, B.H.; Baeg, G.H. Nanotoxicity: An Interplay of Oxidative Stress, Inflammation and Cell Death. *Nanomaterials* **2015**, *5*, 1163–1180. [[CrossRef](#)]
50. Lu, S.; Duffin, R.; Poland, C.; Daly, P.; Murphy, F.; Drost, E.; Macnee, W.; Stone, V.; Donaldson, K. Efficacy of simple short-term in vitro assays for predicting the potential of metal oxide nanoparticles to cause pulmonary inflammation. *Environ. Health Perspect.* **2009**, *117*, 241–247. [[CrossRef](#)]
51. Leppänen, M.; Korpi, A.; Mikkonen, S.; Yli-Pirilä, P.; Lehto, M.; Pylkkänen, L.; Wolff, H.; Kosma, V.-M.; Alenius, H.; Joutsensaari, J.; et al. Inhaled silica-coated TiO<sub>2</sub> nanoparticles induced airway irritation, airflow limitation and inflammation in mice. *Nanotoxicology* **2015**, *9*, 210–218. [[CrossRef](#)]
52. Stocco, A.; Di Bucchianico, S.; Ubaldi, C.; Coppedè, F.; Ponti, J.; Placidi, C.; Blosi, M.; Orтели, S.; Costa, A.L.; Migliore, L. A panel of in vitro tests to evaluate genotoxic and morphological neoplastic transformation potential on Balb/3T3 cells by pristine and remediated titania and zirconia nanoparticles. *Mutagenesis* **2016**, *31*, 511–529. [[CrossRef](#)]
53. Kansara, K.; Patel, P.; Shah, D.; Shukla, R.K.; Singh, S.; Kumar, A.; Dhawan, A. TiO<sub>2</sub> nanoparticles induce DNA double strand breaks and cell cycle arrest in human alveolar cells. *Environ. Mol. Mutagen.* **2015**, *56*, 204–217. [[CrossRef](#)]
54. Patel, P.; Kansara, K.; Senapati, V.A.; Shanker, R.; Dhawan, A.; Kumar, A. Cell cycle dependent cellular uptake of zinc oxide nanoparticles in human epidermal cells. *Mutagenesis* **2016**, *31*, 481–490. [[CrossRef](#)]

55. Wang, Y.; Cui, H.; Zhou, J.; Li, F.; Wang, J.; Chen, M.; Liu, Q. Cytotoxicity, DNA damage, and apoptosis induced by titanium dioxide nanoparticles in human non-small cell lung cancer A549 cells. *Environ. Sci. Pollut. Res.* **2015**, *22*, 5519–5530. [[CrossRef](#)]
56. El-Bassyouni, G.T.; Eshak, M.G.; Barakat, I.A.H.; Khalil, W.K.B. Immunotoxicity evaluation of novel bioactive composites in male mice as promising orthopaedic implants. *Cent. Eur. J. Immunol.* **2017**, *1*, 54–67. [[CrossRef](#)]
57. Schrand, A.M.; Rahman, M.F.; Hussain, S.M.; Schlager, J.J.; Smith, D.A.; Syed, A.F. Metal-based nanoparticles and their toxicity assessment. *Wiley Interdiscip. Rev. Nanomed. Nanobiotechnol.* **2010**, *2*, 544–568. [[CrossRef](#)]
58. Halamoda Kenzaoui, B.; Chapuis Bernasconi, C.; Guney-Ayra, S.; Juillerat-Jeanneret, L. Induction of oxidative stress, lysosome activation and autophagy by nanoparticles in human brain-derived endothelial cells. *Biochem. J.* **2012**, *441*, 813–821. [[CrossRef](#)]
59. Kermanizadeh, A.; Jantzen, K.; Ward, M.B.; Durhuus, J.A.; Juel Rasmussen, L.; Loft, S.; Møller, P. Nanomaterial-induced cell death in pulmonary and hepatic cells following exposure to three different metallic materials: The role of autophagy and apoptosis. *Nanotoxicology* **2017**, *11*, 184–200. [[CrossRef](#)]
60. Klionsky, D.J. Autophagy: From phenomenology to molecular understanding in less than a decade. *Nat. Rev. Mol. Cell Biol.* **2007**, *8*, 931–937. [[CrossRef](#)]
61. Lopes, V.R.; Loitto, V.; Audinot, J.-N.; Bayat, N.; Gutleb, A.C.; Cristobal, S. Dose-dependent autophagic effect of titanium dioxide nanoparticles in human HaCaT cells at non-cytotoxic levels. *J. Nanobiotechnol.* **2016**, *14*, 22. [[CrossRef](#)]
62. Vuong, N.Q.; Goegan, P.; Mohottalage, S.; Breznan, D.; Ariganello, M.; Williams, A.; Elisma, F.; Karthikeyan, S.; Vincent, R.; Kumarathasan, P. Proteomic changes in human lung epithelial cells (A549) in response to carbon black and titanium dioxide exposures. *J. Proteomics* **2016**, *149*, 53–63. [[CrossRef](#)]
63. Soto-Alvaredo, J.; Blanco, E.; Bettmer, J.; Hevia, D.; Sainz, R.M.; López Cháves, C.; Sánchez, C.; Llopis, J.; Sanz-Medel, A.; Montes-Bayón, M. Evaluation of the biological effect of Ti generated debris from metal implants: Ions and nanoparticles. *Metallomics* **2014**, *6*, 1702–1708. [[CrossRef](#)]



© 2019 by the authors. Licensee MDPI, Basel, Switzerland. This article is an open access article distributed under the terms and conditions of the Creative Commons Attribution (CC BY) license (<http://creativecommons.org/licenses/by/4.0/>).